Lag structure of BOLD signals within white matter in resting-state fMRI

Bin Guo[a,b,*], Fugen Zhou[a], Muwei Li[b], John C. Gore[b,c,d,e,f]

[a]Image Processing Center, School of Astronautics, Beihang University, Beijing 100191, Beijing, China

[b]Vanderbilt University Institute of Imaging Science, Vanderbilt University, Nashville, TN 37232, USA

[c]Department of Radiology and Radiological Sciences, Vanderbilt University Medical Center, Nashville, TN 37232, United States

[d]Department of Biomedical Engineering, Vanderbilt University, Nashville, TN 37232, United States

[e]Department of Molecular Physiology and Biophysics, Vanderbilt University, Nashville, TN 37232, United States

[f]Department of Physics and Astronomy, Vanderbilt University, Nashville, TN 37232, United States

Previous studies have demonstrated that BOLD signals in gray matter in resting-state functional MRI (RSfMRI) have variable time lags. We investigated the corresponding variations of signal latencies in white matter within 1393 subjects (both sexes included) from the Brain Genomics Superstruct Project. We divided the dataset into ten equal groups to study both the patterns and reproducibility of latency estimates within white matter. We constructed time delay matrices by computing cross-correlation functions between voxel pairs. Projections of voxel latencies were highly correlated (average Pearson correlation coefficient = 0.89) across the subgroups, confirming the reproducibility and structure of signal lags in white matter. We also applied a clustering analysis to identify functional networks within white matter. Analysis of latencies within and between networks revealed a similar pattern of inter- and intra-network communication to that reported for gray matter. Moreover, a unidirectional path, from inferior to superior regions, of BOLD signal propagation was revealed by higher resolution clustering. The variations of lag structure within white matter are associated with different sensory states (eyes open vs eyes closed, and eyes open with fixation vs. eyes closed). These findings provide additional insight into the character and roles of white matter BOLD signals in brain functions.

Key words: BOLD; fMRI; functional connectivity; resting state; white matter

Significance Statement

Functional MRI (fMRI) has had major impacts on clinical and basic neuroscience, and it has been used extensively to study the functional role and spatiotemporal organization of gray matter in different states. However, functional MRI signals from white matter have usually been ignored or even identified as artifacts. We used fMRI data from 1393 subjects to demonstrate (1) fMRI BOLD signals in white matter are robustly detectable in a resting state and exhibit a reproducible, spatiotemporal organization, similar to gray matter; (2) functional networks within white matter can be obtained by applying clustering analysis on the white matter connectivity matrix; (3) the pattern of signal latencies within and between networks resembles the results for gray matter. Further studies on the Beijing EOEC dataset II also revealed that the variations of latencies within white matter alter with different sensory (visual) states. Our findings demonstrate the that resting-state BOLD signals within white matter should be incorporated into comprehensive models of brain function.

Introduction

Functional magnetic resonance imaging (fMRI) studies were initially based on the detection of changes in blood oxygenation-level dependent (BOLD) signals after a task or stimulus. The technique was later extended to include the detection and analysis of spontaneous signal fluctuations (Fox et al. 2007). Though initially regarded as noise, these spontaneous fluctuations were later analyzed to reveal intrinsic synchronizations of regions within the somatomotor system of the brain (Biswal et al. 1995), and these result in long range, inter-regional low frequency temporal correlations in measured BOLD signals. Conven-

* Corresponding author at: Image Processing Center, School of Astronautics, Beihang University, Beijing 100191, Beijing, China. E-mail: guobin420@gmail.com

tional analyses of these temporal correlations yields a metric widely referred to as functional connectivity (FC) which is derived by assuming exact synchronization of activities and BOLD signals in intrinsic brain networks. However, previous studies in rat and humans found that BOLD fluctuations are spatio-temporally organized across different brain circuits (Majeed et al. 2009; Majeed et al. 2011). To characterize the spatiotemporal patterns of brain activities, Mitra and colleagues recently analyzed inter-regional time latencies or lags in BOLD signals. They derived a time delay matrix from those lags corresponding to extrema in the cross-correlation functions of pairs of voxels. A highly reproducible, state-dependent latency projection (the summed lags relative to other voxels) spanning around 1 second, was found to correspond to spatially segregated functional networks (Mitra et al. 2014, 2015). Since then, much effort has been paid to comprehensively explore lead/lag relationships within the cerebral cortex (Mitra et al. 2014), between the thalamus and the cerebral cortex (Mitra et al. 2015), and the cerebellum (Marek et al. 2018). Such relationships are important for appropriate data analysis and for the interpretation of functional interactions within and between networks.

In direct contrast to studies of BOLD signals in gray matter, BOLD signals in white matter have been ignored for most of the past 30 years and their existence has even been regarded as controversial. In many analyses of fMRI data from gray matter, signals within white matter are treated as nuisance regressors. However, recent growing evidence converges to support the conclusion that fluctuations in white matter BOLD signals encode neural activities (Gawryluk et al. 2014; Grajauskas et al. 2019; Gore et al. 2019), similar to gray matter. It is not clear whether BOLD signals in white matter reflect an intrinsic metabolic demand or are driven by activity in grey matter. Several studies have illustrated the functional role of BOLD signals in white matter. For example, BOLD signals are robustly detectable in WM if appropriate analyses are used; conventional GLM methods throw away sensitivity by using an inappropriate hemodynamic response function (HRF) (Gore et al. 2019; Huang et al. 2018;). Event related measurements show the HRF is different than in GM but can be measured accurately (Li et al., 2019; Wang et al. 2020). WM BOLD activity can be evoked by stimulation in task-specific tracts or regions. The magnitude of WM signals in a task reflects those in GM engaged in the same task, and are modulated by the same factors (Mishra et al, 2020; Li et al, 2020a). At rest, WM tracts show reproducible patterns of connectivity which are summarized in Functional Connectivity Matrices (FCMs) obtained by analyzing resting state correlations between segmented WM and GM parcellations (Ding et al., 2018); the FCM relating WM to GM is altered in various pathologies including Alzheimer's disease in a manner that correlates with behavioral measures (Gao et al., 2020). Distinct, reproducible networks in WM emerge from data-driven analyses in similar manner to cortical circuits (Huang et al., 2020). Moreover, comparisons of partial and full correlations between GM regions with inclusion vs exclusion of WM shows the degree of engagement of specific WM tracts in the couplings between cortical volumes (Li et al., 2020b). Peer and colleagues investigated the functional networks of white matter by applying simple clustering analysis on RSfMRI data of white matter regions (Peer et al. 2017). Highly bilaterally symmetrical functional networks were identified. All these studies and others suggest white matter BOLD signals should be incorporated into models of functional networks.

Despite this converging evidence for the functional role of BOLD signals in white matter, temporal properties of these signals have not been adequately investigated. White matter connects various gray matter areas of the brain to each other, and is responsible for transducing neural activity between regions. In light of recent advances in modelling of how networks communicate (Mishra and Raichle, 2016), examination of the timing relationships within white matter is particularly imperative.

Here we report studies of the latency structure of BOLD signals within white matter. The results are derived from the Brain Genomics Superstruct Project (GSP), a publicly available dataset consisting of a large cohort of healthy young subjects. We found that a highly reproducible latency projection similar to gray matter also exists in white matter. Further latency analysis of inter- and intra-functional networks, identified by clustering on functional connectivity, revealed that some of the functional networks within white matter also exhibit similar spatiotemporal organizations to those in gray matter. Moreover, using the BeijingEOEC dataset II, we found that variations of the lead/lag relationships within white matter were associated with different sensory states of the brain, suggesting a causal effect between them.

Materials and Methods

Subjects and MRI acquisitions. Resting-state data from 1393 healthy subjects (both genders included) were selected from the Brain Genomics Superstruct Project (GSP, Buckner et al 2014). All imaging data were acquired on matched 3T Tim Trio scanners (Siemens Healthcare, Erlangen, Germany) at Harvard University and Massachusetts General Hospital using vendor-supplied 12-channel array head coils. The data for each subject consisted of a 6 minute resting-state echo-planar imaging (EPI) scan with eyes open (38 slices, TR=3s, 3×3×3 mm

isovoxels, interleaved slices) and an MPRAGE anatomical scan (1.2×1.2×1.2 mm resolution).

We further used resting-state data from 20 healthy subjects (11 females) in the BeijingEOEC dataset II (Yan et al., 2009; Zou et al., 2009) to investigate the influence of different sensory states on the lag structure in brain white matter. The following three resting-state sessions were acquired and counterbalanced across the participants: 1) EC (eye closed), 2) EO (eye open), and 3) EOF (eyes open with a fixation). Each of the sessions lasted for eight minutes. During the three resting-state sessions, the participants were instructed to keep as motionless as possible and to think of nothing except for mind wandering. During the EOF session, the participants were instructed to fixate on a black crosshair in the center of a white screen. The functional images were obtained using an EPI sequence with the following parameters: 33 axial slices, thickness/gap=3/0.6 mm, in-plane resolution=64×64, TR=2000 ms, TE=30 ms, flip angle=90º, FOV=200×200 mm. In addition, a T1-weighted sagittal three-dimensional magnetization-prepared rapid gradient echo (MPRAGE) sequence was acquired, covering the entire brain: 128 slices, TR=2530ms, TE=3.39ms, slice thickness=1.33 mm, flip angle=7º, inversion time=1100 ms, FOV=256×256 mm, and in-plane resolution=256×192.

Functional and anatomical preprocessing. All the images were preprocessed using the statistical parametric mapping software package SPM12 (www.fil.ion.ucl.ac.uk/spm/software). First, the images were corrected for slice timing and head motion, and subjects with large head motion (>2 mm in translation or >2° in rotation) were excluded, resulting in a cohort of 1393 subjects. Second, T1-weighted images were segmented into gray matter, white matter, and cerebrospinal fluid using the New Segment utility embedded in SPM12, and all these images were registered to the mean BOLD image output by the motion correction procedure. Third, the BOLD images were normalized into the Montreal Neurological Institute (MNI) space, along with the coregistered T1-weighted images as well as the gray matter and white matter segments. Fourth, linear trends from the BOLD images were removed to correct for signal drifts. Fifth, mean signals from the cerebrospinal fluid mask and whole-brain mask were regressed out as nuisance covariates. After the nuisance regression, the temporal signals were low-pass filtered to retain frequencies between 0.01~0.1Hz. Finally, BOLD images were spatially smoothed with FWHM = 6 mm isotropic Gaussian filter, where smoothing was performed separately on the white matter and the gray matter of each subject, to avoid mixing of signals. To allow for equilibrium to be reached, the initial four time points of each BOLD series were discarded.

Creation of group-level white matter mask. Following the preprocessing, the white matter mask of each subject was normalized to the MNI space and resampled to isotropic resolution of 3 mm. To obtain the masks for group-wise analysis, we used the segments for each subject. Each subject-level white matter mask was generated using a threshold value of 0.95, and the strategy of majority voting was applied to generate the group-level mask. Voxels with a voting rate above 90% were included resulting in a group-level mask consisting of 9321 white matter voxels.

Generation of subject- and group-wise correlation matrix. To reduce the computational demand of calculating correlation matrices, the white matter mask was downsampled using interchanging grids as described previously (Peer et al., 2017; Yeo et al., 2011; Cradock et al., 2012). Briefly, the image slices were alternately sampled by retaining odd and even numbered rows and columns, so that no entire rows or columns of data were missed through slices. For each white matter voxel, the Pearson correlation with all other voxels in the downsampled mask was computed, yielding a whole-brain white matter correlation matrix of size 9321×4654. A group-level correlation matrix was defined to be the average of all the subject-level correlation matrices within the same group.

Construction of white matter functional networks. Functional networks of white matter were identified by clustering voxels on the basis of group-level correlation matrices generated as above (Yeo et al., 2011; Craddock et al., 2012; Blumensath et al., 2013; Moreno-Dominguez et al., 2014; Peer et al., 2017). K-means clustering with correlation as the distance metric and with twelve replicates was performed on the rows of each group-level correlation matrix, which allowed voxels with similar functional connectivity patterns to be grouped into the same cluster. In this study, K-mean clustering was carried out for each subgroup, as well as for the entire dataset by pooling all the subjects together, which served as ground truth.

The cluster similarity between each subgroup and the ground truth was evaluated. We first computed an adjacency matrix, wherein each element in the matrix indicates whether any two voxels are in the same cluster or not, for each clustering result (Peer et al., 2014). We then computed the Dice coefficients between the adjacency matrices from each subgroup and from the entire dataset.

Estimation of time delay between two time series. Given time series of two voxels, $x_1(t)$ and $x_2(t)$, a lagged cross-covariance was computed as,

$$C_{x_1 x_2}(\tau) = \frac{1}{T}\int x_1(t+\tau)\cdot x_2(t)dt$$

where τ is the lag (in units of time), and T is the integration interval, a constant in our experiment. The value of τ at which $C_{x_1 x_2}(\tau)$ exhibiting an extremum defines the temporal lag (delay) between signals x_1 and x_2 (Konig

1994). To determine the lag time value at a temporal resolution finer than the time of repetition, a parabolic interpolation was used, as described previously (Mitra et al., 2014; Laumann et al., 2017; Raut et al., 2020).

Generation of time delay matrix and latency projection. A latency matrix was computed for each subject and then averaged across each group to obtain group-level latencies, a matrix of size 9321×9321. A latency projection was then obtained by averaging over the rows of the latency matrix. The latency projection represents the relative timing of each voxel with respect to the remaining voxels within white matter.

Generation of latency matrices among networks. To characterize the lead/lag relationships among networks, rows and columns of the latency matrix were first rearranged by clusters such that voxels of the same cluster were adjacent to each other, thus subdividing the latency matrix into K×K blocks. Second, intra-network voxels were reordered by their temporal orders deduced from latency projections. Thus, diagonal blocks represent the lead/lag relations between intra-cluster voxels and off-diagonal blocks the lead/lag relations between inter-cluster voxels. Within each block of cluster pairs, the voxels with early timings relative to the remaining voxels in the same block were placed in the upper-left corner and voxels with later timings were placed in the lower-right corner.

State contrast of the latency structure within white matter. We examined statistical differences in the lag structure within white matter among the following three different resting sensory states, i.e., EO, EC, and EOF.

A linear mixed-effects analysis (Chen et al., 2013) was adopted to study the main effect of the sensory states, along with the in-between paired effects. The modeling program, 3dLMEr from AFNI (Cox 1996), was used to build the statistical model, in which variates of sensory states (EO, EC, and EOF), age, and gender were included. Cluster correction was employed for evaluating both main and paired effects. Clusters of statistical significance were identified based on their size. The threshold of cluster size regarded as statistically significant was determined by autocorrelation function modeling combined with a voxel-level threshold of $p < 0.001$. Specifically, we applied 3dFWHMx on preprocessed fMRI data to estimate the parameters of the autocorrelation function (ACF), followed by 3dClustSim for identification of significant cluster-size, within which a corrected significance level was thresholded at $p < 0.05$ and uncorrected voxel-level at $p < 0.001$ (Eklund et al. 2016).

Results

Latency projections in white matter

Voxel-level latency projections. Latency projections within WM derived from the GSP dataset are shown in Figure 1. The latencies ranged from -0.1 s to 0.1 s, with positive values indicating lags and negative values leads in in timings of signal propagations. It can be seen that the distribution of the latencies was highly bilaterally symmetric. The white matter regions with the smallest and greatest lag values were the internal capsule (IC) and the posterior corona radiate (PCR), respectively. A gradual increase in lag value from the posterior thalamic radiation (PTR) to the optic radiation (OR) was also observed. The correlogram in Figure 1-B shows the pair-wise correlation coefficient (CC) among the ten separate subgroups. The CC value ranged from 0.859 to 0.908, which demonstrates high spatial similarities in latency projections across subgroups.

Tests with spatially randomized white matter voxels. To examine whether the observed latency projection patterns were obtained by chance, one group of subjects was randomly selected and the spatial locations of time series in white matter were randomly permuted. Group-level latency projections were computed using the procedure described before, with results shown in Figure S7-A. Overall, though the resulting latencies ranged from -0.05 s to 0.05 s, most latencies were near zero, which can be seen in the histogram in Figure S7-B. Compared to Figure 1, the distribution of latency projections tended to lose spatial coherence, indicating no spatiotemporal organization in the randomized white matter and thus confirming that the latency projections observed in Figure 1-A were driven by intrinsic spatial organizations.

Tests with temporally randomized white matter time series. To examine whether the observed latency projection patterns resulted from intrinsic temporal coherences in white matter signals, the temporal order of time series of all white matter voxels was randomly shuffled, from which group-level latency projections were computed for each subgroup. Though the latency projections derived as such also exhibited lead/lag relationships (see Figure S8-A), the lag range was reduced to -0.02 ~ 0.02 s with haphazard spatial patterns that bore no clear relations to the underlying white matter bundles. Moreover, between-group CC decreased to nearly zero (0.035 ± 0.032), indicating that spatial consistencies across subjects were virtually lost (see Figure S8-B).

Functional networks and latency matrix

Functional networks within white matter. Functional networks within white matter identified by using K-means clustering are shown in Figure 2. It can be seen from Figure 2A that as the number of clusters K increases, the Dice coefficients tend to decrease. The numbers of clusters that yield the most stable cluster segregations are 2, 4, 8, and 13 (denoted as asterisks in Figure 2A). These clusters are visualized in left, right, front and back views in Figure 2B.

Latency matrices among white matter functional networks. We examined lead/lag relationships among white matter functional networks (WMFN) on different numbers of clusters in a coarse-to-fine manner. Here the

latency matrices of only 2, 4, and 8 clusters are shown in Figures 3-5, with diagonal blocks representing intra-network lead/lag relationships, while off-diagonal blocks inter-network lead/lag relationships.

Lead/lag relationships at the coarsest level (K=2) of clustering are shown in Figure 3, in which the two networks clustered were in the top (green colored) and bottom (red colored) portions of the brain respectively. Note that a portion of the anterior corpus callosum was clustered into the bottom cluster. For the top cluster, a pattern ordering the intra-network latencies was readily identified. This latency pattern resembles previous studies on functional networks of gray matter (Mitra et al, 2015), indicating similar spatiotemporal properties such that the the top cluster appeared to contain temporally well-ordered early, medium and late components within WMFN. Meanwhile, for the bottom cluster, a reverse pattern to the top cluster's intra-network lead/lad relationship was observed, indicating a reverse temporal ordering derived from the lag projection. For inter-network lead/lag relationship, the latency patterns in the off-diagonal blocks were quite different from that found in gray matter previously. Part of the early voxels from the top cluster lag part of the early voxels from the bottom cluster.

Clusters with K=4 are shown in Figure 4. It can be seen that there were well-ordered distributions of inter- and intra-network latencies between network 3 (blue) and network 4 (yellow), indicating the existence of reciprocal inter- and intra-network timings. At this clustering resolution, network 2 (green) exhibited a clear reverse intra-network temporal order against the temporal order deduced from the latency projections. In network 1 (red), the overall temporal order was unclear though some of the voxels led some of the voxels from other clusters.

Clusters with K=8 are shown in Figure 5, in which reciprocal inter- and intra-network propagations were observed among the lower-right blocks consisting of network 5 (cyan), 6 (purple), 7 (antique white), and 8 (midnight blue), but no temporal relationships were clearly visible between network 4 (yellow) and other networks except network 1 (red). Network 2 consisted of a major portion of the corpus callosum, the temporal relationships of which with network 4 seemed disordered. While further investigations into temporal relationships between networks 2 and 4 are warranted, the inter-network lead/lag relationship of network 2 and networks 5-8 tended to signify a pattern of signal propagations from network 2 to the other four networks. A similar phenomenon was also observed for network 1. First of all, network 3 (medium blue) led network 1, indicating a unidirectional path of signal propagation from network 3 to network 1. At the same time, networks 5-8 appeared to lag network 1, suggesting a unidirectional path of signal propagation from network 1 to the other four networks. In summary, at this clustering resolution, unidirectional paths, i.e. from bottom to top, of signal propagations could be identified (Figure 5-C). Latency matrices of other clusters are provided in Figures S1~S6 in the Supplementary Material.

Latency projections of different sensory states

Latency projections obtained during different sensory states are shown in Figure 6. As can be seen, the spatial patterns of latency projections in white matter were largely preserved across different sensory states, which were also reminiscent of those obtained from the GSP dataset in Figure 1. Pearson's correlation analysis showed that the CC between EO and EC, EO and EOF, and EC and EOF were 0.798, 0.805 and 0.809 respectively. Close inspections revealed that, for all the three states, voxels with large lag values were mostly distributed in the corona radiata (CR), OR, and the four corners of ventricles, whereas voxels with small lag values were mainly concentrated around the IC. Notable differences in lag values among the three sensory states, however, were also clearly visible, especially in the IC and OR. Larger lag values tended to be concentrated around the OR for EC as compared with EO and EOF, while small lag magnitudes tended to be around the IC for EO and EOF.

Figure 7 shows the regions that exhibited significant differences among the three different states (defined by FWE-corrected $p<0.05$ and uncorrected $p<0.001$ for both main effect and paired effect). One prominent cluster was observed in the IC and another in the OR. Post hoc t-tests suggest a change of lag within these two regions between different sensory states, EC vs. EO (Figure 6-B), and EC vs. EOF (Figure 6-C). However, no significant effect was observed between EO and EOF (Figure 6-D).

Figure 8 shows the change of latency within regions showing significant effects. As compared with EC, the most prominent change in latency with eyes open was a shift toward later values in the IC, while reverse changes, shifting toward earlier values, were observed in the OR (Figure 7-A, B). Similar changes were also observed by contrasting EC with EOF (Figure 7-C, D). Despite the gross spatial similarity of latency projections seen in Figure 6, the lag values within regions of significant effects changed reliably across different paired sensory states. Specifically, lag values within regions of significant effect changed from -0.46s~0.44s for EC to -0.16s~0.17s for EO, and lag values within regions of significant effect changed from -0.46s~0s (in EC) to -0.14s~0.07s (in EOF).

Discussion

We have described how latency projections (Nikolic 2007) derived from time delay matrices were used to investigate the BOLD lag structure within white matter. The consistency of latency projections across ten subgroups consisting of large cohorts of younger healthy subjects attest to the high stability and reproducibility of the lag structure within white matter that is similar to gray matter. We also

investigated white matter functional networks by applying a clustering technique on functional connectivity matrices. Reproducible functional networks across the ten subgroups were obtained. We further explored how these spatially segregated functional networks are integrated with each other by analyzing inter- and intra-network lead/lag relationships. While some of the networks exhibited reciprocal in-between communication patterns, network-wise lead/lag relations, not reported in gray matter, were also revealed. A unidirectional propagation path of BOLD signals was identified from lead/lag analysis of higher resolution functional networks derived from finer grained clustering. We also examined the effects of different sensory states (EO, EC, EOF) to find out whether the latency structure was associated with specific neural inputs. Statistical analysis revealed appropriately localized differences between EO/EC, and between EOF/EC, suggesting that the latency structure in white matter is affected by task-related neural activity.

White matter functional networks

A previous study (Peer et al. 2017) demonstrated the high reproducibility of bilaterally symmetrical WMFNs. We validated this finding with a much larger dataset. Bilaterally symmetrical WMFNs were also identified in our experiments. However, in the work of Peer et al., the identified WMFNs were organized into three layers (superficial, middle, and deep) with each directly overlaying the preceding one. This spatial overlapping was not observed in this study as our subject-level and subsequent group-level WM masks were generated by highly conservative thresholding ($\geq$0.95). As there are lingering concerns that WM BOLD signals may arise from the effects of partial volume averaging with adjacent GM and vasculature, such a tight threshold minimized this potential confound.

Historically, rsfMRI has been extensively used to identify functional networks in the cortex (Yeo et al. 2011; Power et al. 2011). Here we complement previous studies by examining apparent functional networks in white matter. Our results expand beyond previous studies on WMFNs by using a much larger dataset and by quantifying the specific timings of BOLD signals throughout the brain.

Latency of intra- and inter-networks

Intra- and inter-network lead/lag measurements have been analyzed to describe the temporal relationships between spatially segregated resting state networks (RSNs) of gray matter (Mitra et al. 2014). Studies in human (Mitra et al. 2015; Mitra et al. 2014) and mice (Matsui et al. 2016) have reported that BOLD signals propagate through the cerebral cortex along stereotypical spatiotemporal sequences to give rise to the network-level organization.

In WM, three observations can be derived from network-level latency analyses.

First, some WMFNs exhibited similar intra- and inter-network latency patterns to gray matter (indicated by yellow boxes in Figure 3, 4, 5), suggesting similar spatiotemporal organizational principles govern these networks. For diagonal blocks, this pattern illustrates that each network has early, middle, and late components. With respect to off-diagonal blocks, this pattern represents reciprocal communication between paired networks with no network leading or following the other. Building on a previous study of WMFNs (Peer et al. 2017), our findings reveal the spatiotemporal organization across FNs. Future studies could explore factors that affect these results including the influences of different diseases on the functional integration of WMFNs.

Second, temporal orders within some networks (indicated by red boxes in Figure 3, 4, 5) are dominated by the temporal order deduced from the latency projection. Each latency block is reordered according to the temporal order obtained from the latency projection. Ideally, if the temporal order within each latency block is consistent with that deduced from the latency projection, which encompasses the global temporal order within white matter, large lags will be uniformly distributed in the top and right position of each latency block. However, these networks turned out to exhibit a reverse temporal order. These regions consist mainly of IC and the anterior part of corpus callosum (network 2 in Figure 3). Further investigations are warranted for proper explanation of this observation.

Third, a unidirectional propagation of BOLD signals within white matter can be identified, which suggests that most of the BOLD signals propagate along this path. This unidirectional path of propagation may imply that the there is a continuous flow of information through the brain during the resting-state. Future experiments on joint latency analysis, combining both white matter and gray matter, may help explain this.

Influences of different sensory states on white matter latency structure

Given the observed effects of different sensory states on latency, it is reasonable to infer that these effects are potentially of neurophysiological origin. Though latency projections from different sensory states exhibited similar tendency of increasing lag values along OR, lag values changed significantly when contrasting EO with EC, and also EOF with EC. While comparisons between EO and EOF showed no significant changes in OR, WM BOLD signals in OR show close associations with visual tasks (Ding et al. 2016; Ding et al. 2018; Li et al. 2019). Ding et al. also found that visual stimulations significantly enhance the correlation between gray matter and OR (Ding et al. 2018), which may explain the lower estimated lag values in OR. The change of lag values due to different sensory states may suggest a different extent of engagement of OR, in which a smaller lag value in OR corresponds to more active engagement of OR in modulating visual information. Likewise, explanations may extend to the IC as well, as it consists of both ascending and descending fibers. This structure, situated close to the thalamus, routes information

up to the corona radiata and down to the pons. If the IC is more actively engaged in a task, the time delays within the affected region may be shortened.

Latency structure of white matter in relation to vascular physiology

BOLD signals result from variations of regional blood concentrations of oxy- and deoxy-hemoglobin. Hence the latency structure may be determined by the anatomy of the venous drainage system within white matter. Previously in gray matter, the venous drainage system was shown to be not relevant to the latency structure (Mitra et al. 2014). Indeed, for gray matter, the superficial venous system drains into the superior sagittal sinus from an inferior to superior direction, while the superior sagittal sinus drains the venous blood from superior to inferior regions. However, the distribution of the lag values does not follow the flow direction of the superficial venous drainage system, which therefore rules out the possibility that the latency structure merely reflects the vascular architecture. Likewise, generally in white matter, the deep venous drainage system removes venous blood from anterior (via the inferior sagittal sinus, the internal cerebral vein, and the basal vein) to posterior (the straight sinus, the great cerebral vein) directions. Again, the distribution of the lag values within white matter are inconsistent with this flow. From our analyses a unidirectional path of BOLD signal propagation was revealed, from inferior to superior. Moreover, the lag values in the IC and the OR were significantly associated with different sensory states, which is not explicable in terms of the deep venous drainage system.

As we based our study on fMRI BOLD signals, we cannot exclude hemodynamic effects on latency projections. Variations during different sensory states in the latency structure could be due to changes in regional neurovascular couplings. However, we can explore the possible variances of the latency matrix that can be explained by hemodynamic effects by applying PCA analysis on the latency matrix of each group. Briefly, PCA analysis was performed on a sub-sampled latency matrix, with columns of voxels from the down-sampled white matter mask, as used in clustering analysis. Similar analysis was performed to identify 8 threads propagating within gray matter (Mitra A et al. 2015b). Eigenspectra of latency matrices from subgroups showed highly similar distributions (Refer to Figure S9 for the distribution the eigenspectra). On average, the principle component with the largest eigenvalue can account for only 12% of the variance of the latency matrix, leaving a large part to be explained by other possible factors.

Acknowledgments

We sincerely thank Dr. Zhaohua Ding for his insights in our discussion.

References

Biswal, B., Zerrin Yetkin, F., Haughton, V. M., & Hyde, J. S. (1995). Functional connectivity in the motor cortex of resting human brain using echo-planar MRI. Magnetic resonance in medicine, 34(4), 537-541.

Blumensath T, Jbabdi S, Glasser MF, Van Essen DC, Ugurbil K, Behrens TE, Smith SM (2013) Spatially constrained hierarchical parcellation of the brain with resting-state fMRI. Neuroimage 76:313–324

Buckner R. L., Krienen F. M., Castellanos A., Diaz J. C., Yeo B. T. (2011). The organization of the human cerebellum estimated by intrinsic functional connectivity. Journal of neurophysiology.

Chen G, Saad Z., Britton J.C., Pine D.S., Cox R.W. (2013) Linear mixed-effects modeling approach to FMRI group analysis. Neuroimage 73, 176–190

Cox, R. W. (1996). AFNI: Software for analysis and visualization of functional magnetic resonance neuroimages. Computers and Biomedical Research, 29(3), 162–173.

Craddock RC, James GA, Holtzheimer PE 3rd, Hu XP, Mayberg HS (2012) A whole-brain fMRI atlas generated via spatially constrained spectral clustering. Hum Brain Mapp 33:1914–1928

Ding Z., Huang, Y., Bailey, S. K., et al. (2018). Detection of synchronous brain activity in white matter tracts at rest and under functional loading. Proceedings of the National Academy of Sciences, 115(3), 595-600.

Ding Z, Xu R, Bailey SK, Wu TL, Morgan VL, Cutting LE, Anderson AW, Gore JC (2016) Visualizing functional pathways in the human brain using correlation tensors and magnetic resonance imaging. Magn Reson Imaging 34:8–17.

Eklund, A., Nichols, T. E., & Knutsson, H. (2016). Cluster failure: Why fMRI inferences for spatial extent have inflated false-positive rates. Proceedings of the National Academy of Sciences of the United States of America, 113(28), 7900–7905.

Fox M. D., Raichle M. E. (2007). Spontaneous fluctuations in brain activity observed with functional magnetic resonance imaging. Nature reviews neuroscience, 8(9), 700-711.

Gao Y, Sengupta A, Li M, et al. (2020) Functional connectivity of white matter as a biomarker of cognitive decline in Alzheimer's disease. Plos one, 15(10): e0240513.

Gawryluk J. R., Mazerolle E. L., D'Arcy R. C. (2014). Does functional MRI detect activation in white matter? A review of emerging evidence, issues, and future directions. Frontiers in neuroscience, 8, 239.

Gore J. C., Li M., Gao Y., Wu T. L., Schilling K. G., Huang Y., Anderson A. W. (2019). Functional MRI and resting state connectivity in white matter-a mini-review. Magnetic resonance imaging, 63, 1-11.

Grajauskas L. A., Frizzell T., Song X., D'Arcy R. C. (2019). White matter fMRI activation cannot be treated as a nuisance regressor: Overcoming a historical blind spot. Frontiers in neuroscience, 13, 1024.

Huang Y, Bailey SK, Wang P, Cutting LE, Gore JC, Ding Z. (2018) Voxel-wise detection of functional networks in white matter. Neuroimage.183:544-552.

Huang Y, Yang Y, Hao L, et al. (2020) Detection of functional networks within white matter using independent component analysis. NeuroImage, 222: 117278.

König P. (1994) A method for the quantification of synchrony and oscillatory properties of neuronal activity. J Neurosci Methods. 54:31-37.

Laumann TO, Snyder AZ, Mitra A, et al. (2017) On the stability of BOLD fMRI correlations. Cerebral cortex. 27(10): 4719-4732.

Li M., Newton A. T., Anderson A. W., Ding Z., Gore J. C. (2019). Characterization of the hemodynamic response function in white matter tracts for event-related fMRI. Nature communications, 10(1), 1-11.

Li M, Ding Z, Gore J C. (2020) Identification of White Matter Networks Engaged in Object (Face) Recognition Showing Differential Responses to Modulated Stimulus Strength. Cerebral cortex communications, 1(1): tgaa067.

Li M., Gao Y., Gao F., Anderson A. W., Ding Z., Gore J. C. (2020). Functional engagement of white matter in resting-state brain networks. NeuroImage, 220, 117096.

Majeed W., Magnuson M., Keilholz S. D. (2009). Spatiotemporal dynamics of low frequency fluctuations in BOLD fMRI of the rat. Journal of Magnetic Resonance Imaging: An Official Journal of the International Society for Magnetic Resonance in Medicine, 30(2), 384-393.

Majeed W., Magnuson M., Hasenkamp W., Schwarb H., Schumacher E. H., Barsalou L., Keilholz S. D. (2011). Spatiotemporal dynamics of low frequency BOLD fluctuations in rats and humans. Neuroimage, 54(2), 1140-1150.

Marek S., Siegel J. S., Gordon E. M., Raut R. V., Gratton C., Newbold D. J., et al, A. (2018). Spatial and temporal organization of the individual human cerebellum. Neuron, 100(4), 977-993.

Matsui T, Murakami T, and Ohki K. (2016) Transient neuronal coactivations embedded in globally propagating waves underlie resting-state functional connectivity. Proc Natl Acad Sci USA 113: 6556-6561.

Mishra A, Li M, Anderson A W, et al. (2020) Concomitant modulation of BOLD responses in white matter pathways and cortex. NeuroImage, 216: 116791.

Mitra A, Snyder AZ, Hacker CD, Raichle ME (2014) Lag structure in resting-state fMRI. Journal of Neurophysiology. 111(11): 2374-2391.

Mitra A, Snyder A Z, Blazey T, et al. (2015) Lag threads organize the brain's intrinsic activity. Proceedings of the National Academy of Sciences, 112(17): E2235-E2244.

Mitra, A., Snyder, A. Z., Tagliazucchi, E., Laufs, H., Raichle, M. E. (2015). Propagated infra-slow intrinsic brain activity reorganizes across wake and slow wave sleep. Elife, 4, e10781.

Moreno-Dominguez D, Anwander A, Knosche TR (2014) A hierarchical method for whole-brain connectivity-based parcellation. Hum Brain Mapp 35:5000–5025

Nikolic D. (2007) Non-parametric detection of temporal order across pairwise measurements of time delays. J Comput Neurosci 22: 5-19.

Peer M, Nitzan M, Bick AS, Levin N, Arzy S. (2017) Evidence for Functional Networks within the Human Brain's White Matter. J Neurosci. 37(27):6394-6407.

Peer M, Nitzan M, Goldberg I, Katz J, Gomori JM, Ben-Hur T, Arzy S (2014) Reversible functional connectivity disturbances during transient global amnesia. Ann Neurol 75:634–643

Pellerin L, Magistretti PJ. 2004. Let there be (NADH) light. Science 305:50–52

Power J. D., Cohen A. L., Nelson S. M., et al. (2011). Functional network organization of the human brain. Neuron, 72(4), 665-678.

Raichle M. E., MacLeod A. M., Snyder A. Z., Powers W. J., Gusnard D. A., Shulman G. L. (2001). A default mode of brain function. Proceedings of the National Academy of Sciences, 98(2), 676-682.

Raichle M. E., Mintun M. A. (2006). Brain work and brain imaging. Annu. Rev. Neurosci., 29, 449-476.

Raichle M. E. (2015) The restless brain: how intrinsic activity organizes brain functionPhil. Trans. R. Soc. B37020140172

Raut R. V., Mitra A., Snyder A. Z., Raichle M. E. (2019). On time delay estimation and sampling error in resting-state fMRI. Neuroimage, 194, 211-227.

Sun F. T., Miller L. M., D'Esposito M. (2005) Measuring temporal dynamics of functional networks using phase spectrum of fMRI data. Neuroimage, 28(1), 227-237.

Wang T., Wilkes D. M., Li M., Wu X., Gore J. C., Ding Z. (2020). Hemodynamic response function in brain white matter in a resting state. Cerebral cortex communications, 1(1), tgaa056.

Yan C., Liu D., He Y., Zou Q., Zhu C., Zuo X., Long X., Zang Y. (2009) Spontaneous brain activity in the default mode network is sensitive to different resting-state conditions with limited cognitive load. PLoS ONE 4, e5743.

Yeo BT, Krienen FM, Sepulcre J, Sabuncu MR, Lashkari D, Hollinshead M, Roffman JL, Smoller JW, Zollei L, Polimeni JR, Fischl B, Liu H, Buckner RL (2011) The organization of the human cerebral cortex estimated by intrinsic functional connectivity. JNeurophysiol106:1125–1165

Zou Q., Long X., Zuo X., Yan C., Zhu C., Yang Y., Liu D., He Y., Zang Y. (2009) Functional connectivity between the thalamus and visual cortex under eyes closed and eyes open conditions: A resting-state fMRI study. Hum Brain Mapp 30, 3066-3078.

Figure 1 Latency projections and inter-group correlations obtained in GSP dataset. The 1393 subjects chosen were randomly divided into ten subgroups of approximately 140 subjects. (A) Voxel-wise latency projections of TD obtained from the first group within white matter. (B) Pair-wise spatial correlations in latency projections between the ten subgroups studied. The mean and standard deviation within the upper triangular region, demarcated by the blue triangle, of the correlogram are 0.887 and 0.013, respectively).

Figure 2 Variations of clusters obtained from white matter correlation matrix with values of K. (A) Average Dice Coefficients over the 10 subgroups, with asterisks denoting local maxima. (B) From top to bottom are 2, 4, 8 and 13 functional networks clustered from white matter correlation matrix. Highly bilaterally symmetrical functional networks are observed.

Figure 3 Intra- and inter-network lead/lag relations on two clusters. (A) The intra- and inter-network lead/lag array. (B) The left and front view of the clustering results. Blocks referred to in the Section of Discussion are outlined in different colors.

Figure 4 Intra- and inter-network lead/lag analysis on four clusters. (A) The intra- and inter-network lead/lag array. (B) The left and front view of the clustering results. Blocks referred to in the Section of Discussion are outlined in different colors.

Figure 5 Intra- and inter-network lead/lag analysis on eight clusters. (A) The intra- and inter-network lead/lag array. (B) The left and front view of the clustering results. Blocks referred to in the Section of Discussion are outlined in different color. (C) The unidirectional path identified from the latency matrix at this clustering resolution. Large arrow width corresponds to major part of the cluster. An arrow from network 6 to network 8 with larger width than the reverse arrow (network 8 to network 6) indicates that major part of network 6 leads network 8, as can be observed in the (6, 8) latency block of the latency matrix. Blocks referred to in the section of Discussion are outlined in different colors.

Figure 6 Latency projections in white matter obtained in the Beijing EOEC dataset II. (A) EC. (B) EO. (C) EOF. Note that the distributions patterns across the three different states are grossly consistent.

Figure 7 Distributions of white matter voxels with significant effects among different sensory states. (A) Main effect (mixed effect). (B) Paired effect of EC and EO. (C) Paired effect of EC and EOF.

Figure 8 Distributions of latencies in white matter with significant paired effect. (A) EC (top panel) vs. EO (bottom panel). (B) EC (top panel) vs. EOF (bottom panel).

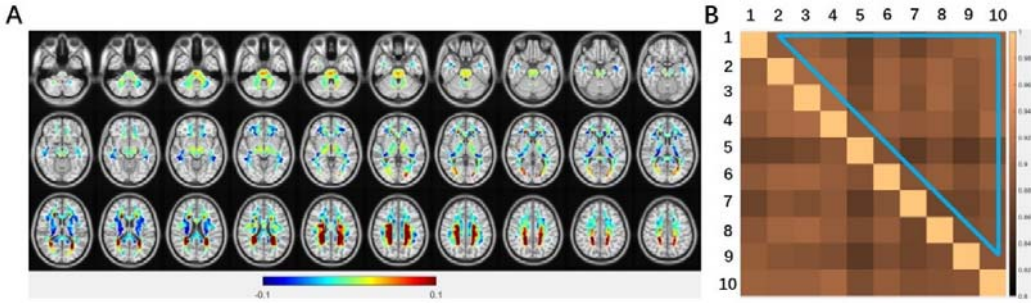

Figure 1

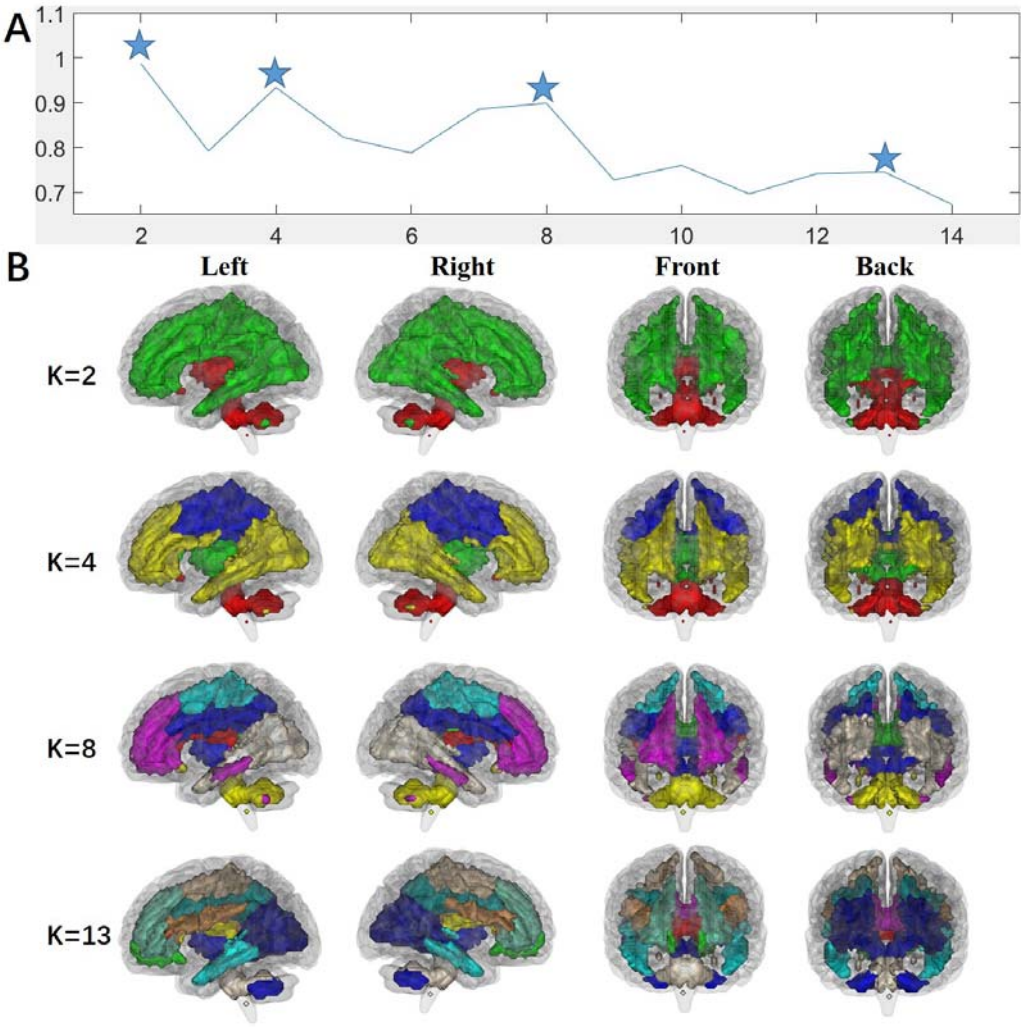

Figure 2

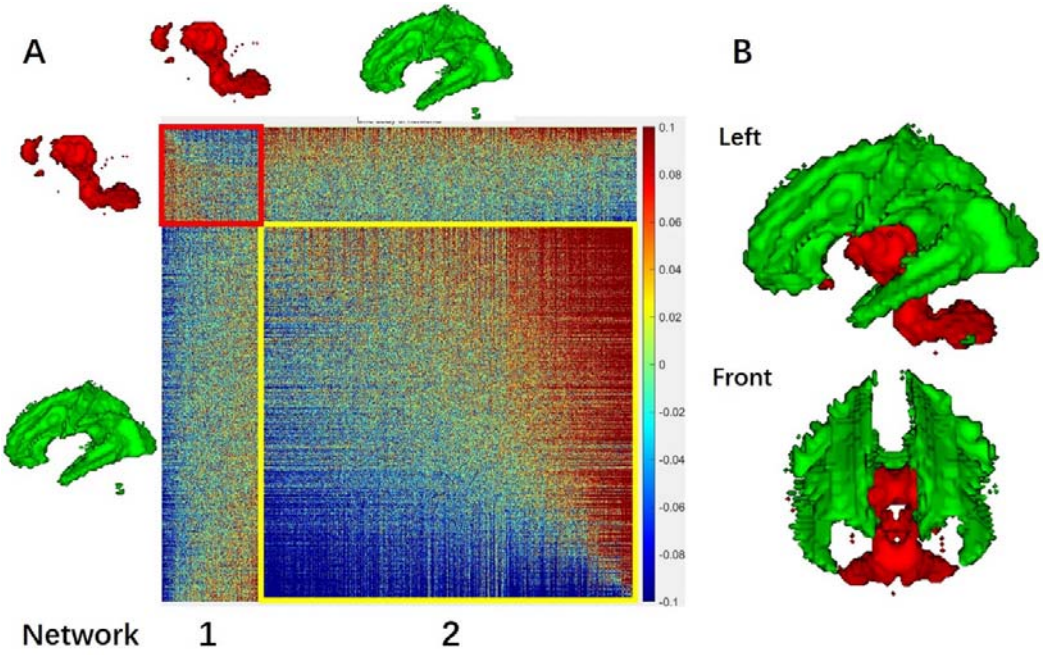

Figure 3

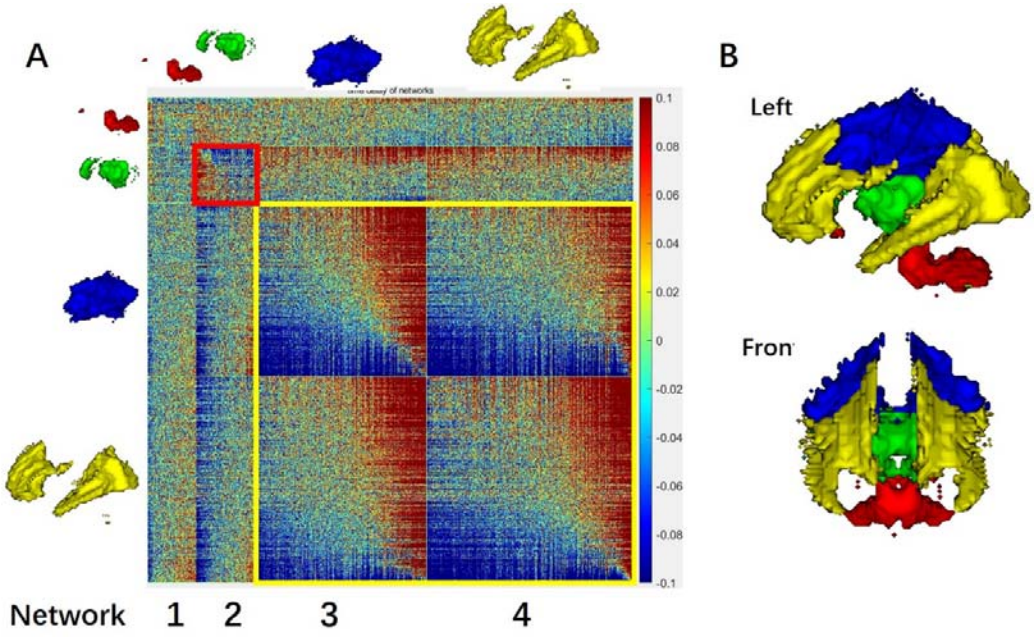
A
B
Left
Fron
Network
1
2
3
4
0.1
0.08
0.06
0.04
0.02
0
-0.02
-0.04
-0.06
-0.08
-0.1

Figure 4

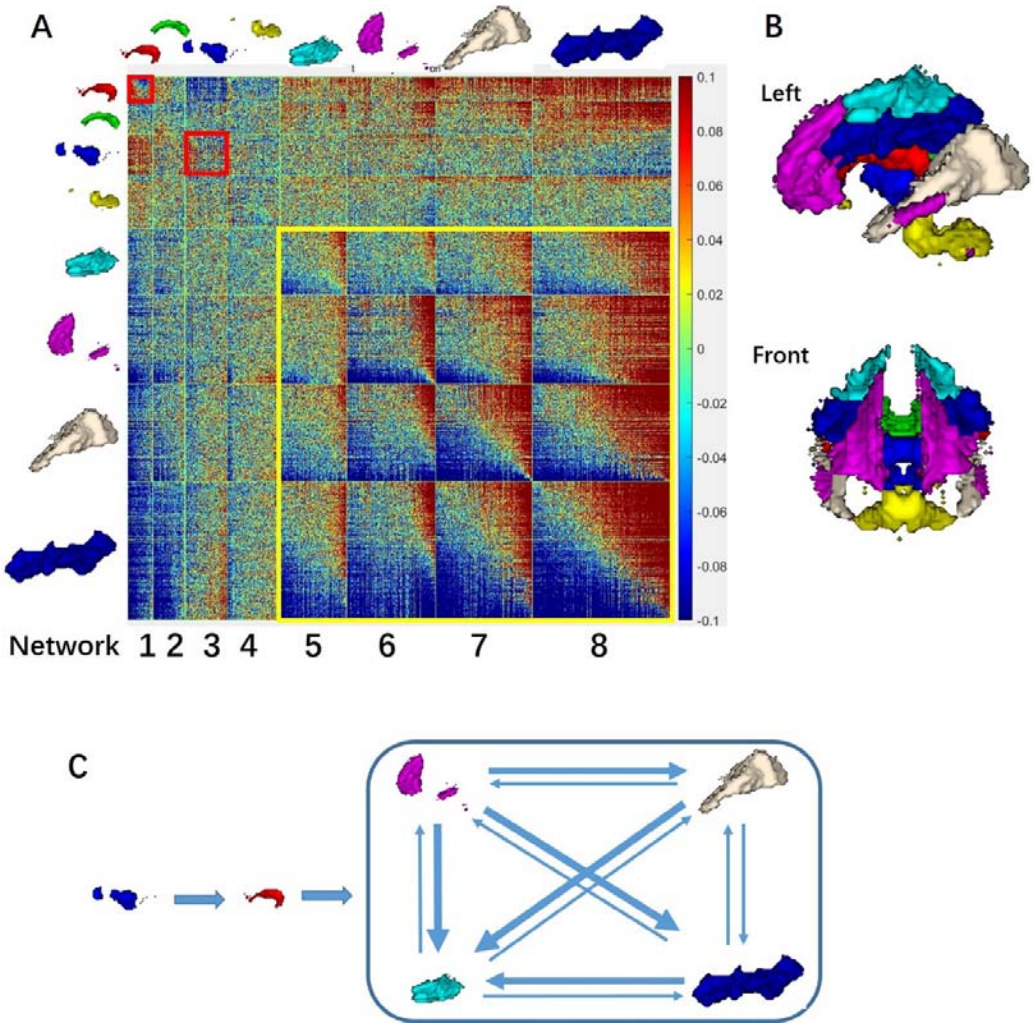
A
B
Left
Front
C
Network 1 2 3 4 5 6 7 8
0.1
0.08
0.06
0.04
0.02
0
-0.02
-0.04
-0.06
-0.08
-0.1

Figure 5

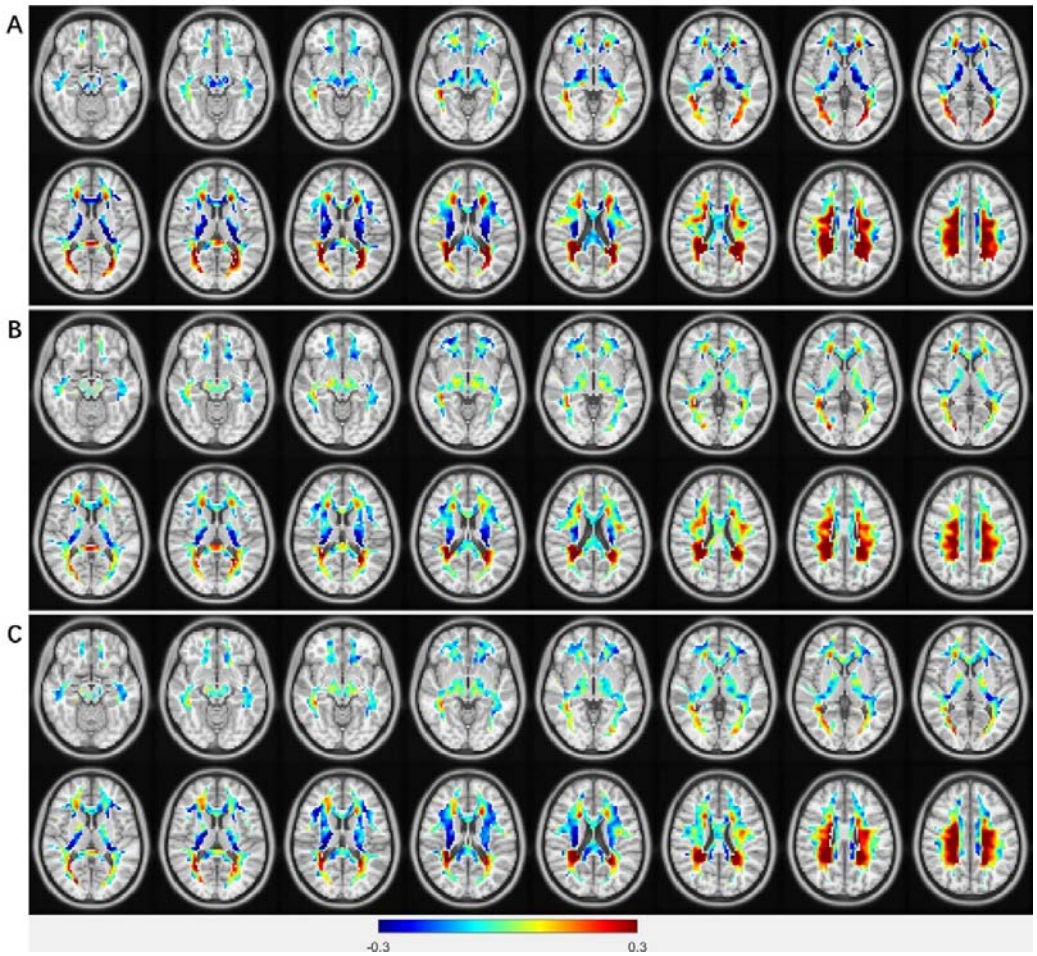

Figure 6

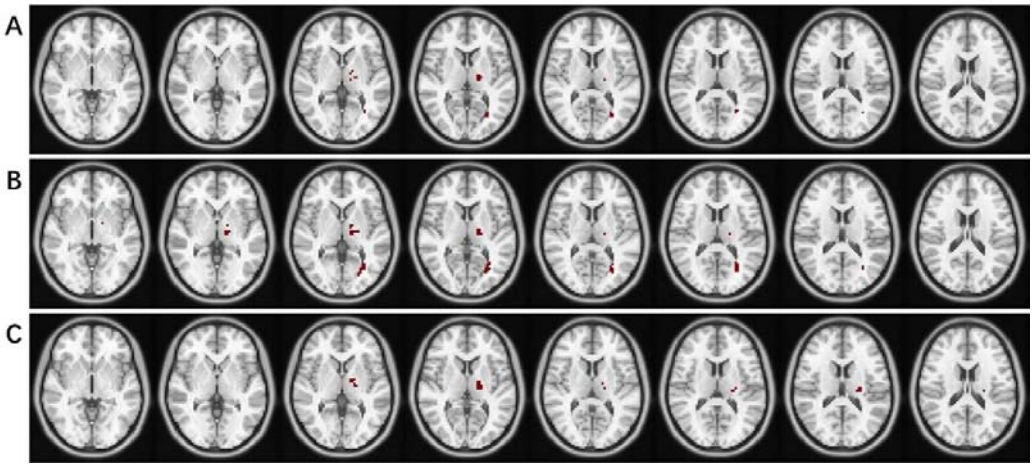

Figure 7

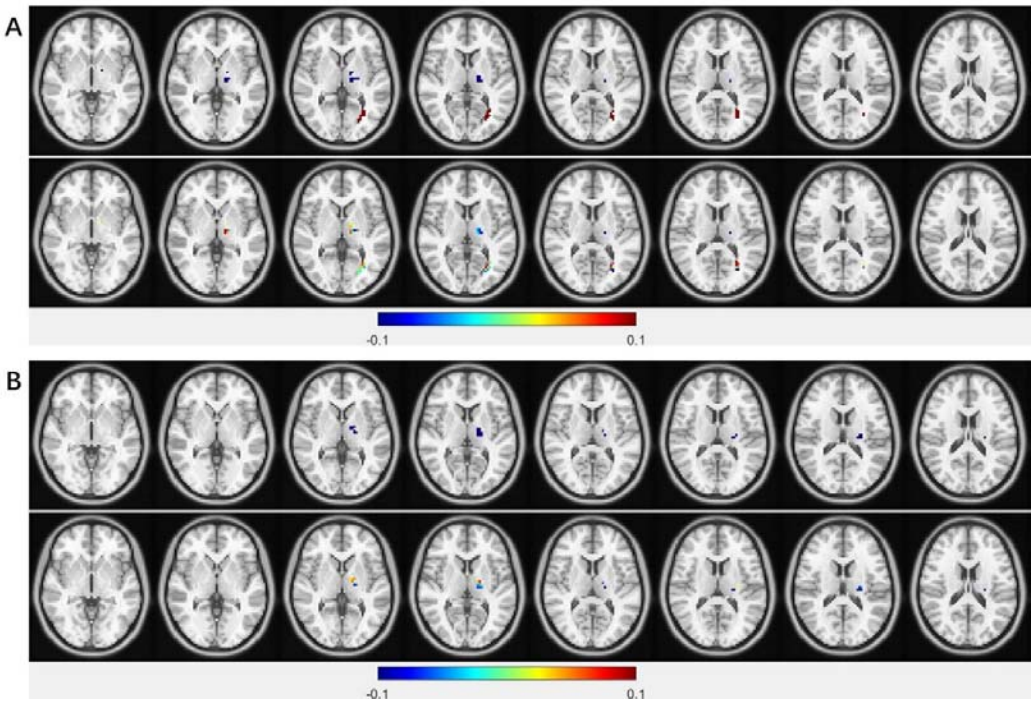

Figure 8